Nickel and Cobalt Hexamethylentetramine Complexes (NO$_3$)$_2$Me(H$_2$O)$_6$(HMTA)$_2$·4H$_2$O (Me = Co^{2+}, Ni^{2+}): New Molecular Precursors for the Preparation of Metal Dispersions

Pavel Afanasiev,[*,†] **Sandra Chouzier,**[†] **Tivadar Czeri,**[‡] **Guillaume Pilet,**[§] **Christophe Pichon,**[‡] **Magalie Roy,**[‡] **and Michel Vrinat**[†]

Institut de Recherche sur la Catalyse et Environnement, Université de Lyon 1, 2 Avenue A. Einstein, 69626 Villeurbanne Cédex, France, Institut Français du Pétrole, IFP-Lyon, BP 3, 69390 Vernaison, France, and Groupe de Cristallographie et Ingénierie Moléculaire, Laboratoire des Multimatériaux, UMR 5615 CNRS, Université de Lyon 1, Campus de la Doua, 69622 Villeurbanne Cédex, France

Nickel and cobalt hexamethylenetetramine (HMTA) complexes (NO$_3$)$_2$Me(H$_2$O)$_6$(HMTA)$_2$·4H$_2$O were prepared and characterized structurally by single-crystal X-ray diffraction. Both compounds crystallize in the triclinic $P\bar{1}$ space group with the same structure. The structures are three-dimensional hydrogen-bonded supramolecular frameworks containing two-dimensional cationic assemblies connected with proton acceptors, which are noncoordinated anionic species (nitrate) and neutral HMTA molecules. Thermal decomposition of these compounds under an inert atmosphere leads to the high-surface-area metal−carbon foams containing nickel and cobalt nanoparticles embedded within onionlike carbon shells. The decomposition process as studied by thermal analysis and in situ X-ray absorption spectroscopy (XAS) measurements occurs as a rapid loss of oxygen in the form of CO, beginning at temperatures as low as 323 K. As the in situ XAS study demonstrated, the evolution of nickel and cobalt coordination spheres occurs with intermediate formation of amorphous metal carbides, which subsequently decompose to the metal nanoparticles covered with carbon shells.

1. Introduction

Porous materials with hierarchical pore systems attract great interest in researchers.[1,2] Spongelike or foamlike structures consisting of nanoparticles are eminently appropriate for applications where a large surface area is needed, such as electrochemistry or catalysts. Polymodal pore structure allows optimization of the relationship between the chemical reaction and the mass transfer from the solid surface to the volume of the reactants and vice versa. Nickel and cobalt are well-known magnetic materials, whereas nanoparticles of these metals are widely used in the actual catalytic studies on newly developed processes such as

biomass gasification or hydrodechlorination.[3,4] In the last few years, considerable research activity was targeted on the preparation of nanoscopic nickel and cobalt, using various physical or chemical methods.[5–8]

Hexamethylenetetramine (HMTA) easily forms stoichiometric molecular compounds with transition metals, which can be conveniently used for the preparations of inorganic materials by decomposition. Recently, a molybdate HMTA complex has been prepared, whose decomposition in an inert atmosphere leads to the dispersed Mo$_2$N nitride[9] and then is extended to the ternary (Ni) Co−Mo nitrides. In the course of these studies, we observed that decomposition of mono-

* To whom correspondence should be addressed. E-mail: pavel.afanasiev@ircelyon.univ-lyon1.fr.
† Institut de Recherche sur la Catalyse et Environnement, Université de Lyon 1.
‡ Institut Français du Pétrole, IFP-Lyon.
§ UMR 5615 CNRS, Université de Lyon 1.

(1) Kuang, D.; Brezesinski, T.; Smarsly, B. *J. Am. Chem. Soc.* **2004**, *126*, 10534.
(2) Ding, Y.; Erlebacher, J. *J. Am. Chem. Soc.* **2003**, *125*, 7772.
(3) Furusawa, T.; Tsutsumi, A. *Appl. Catal.* **2005**, *278*, 195.
(4) Keane, M. A.; Patterson, P. M. *Catal. Lett.,* **2005**, *99*, 33.
(5) Yamamoto, K.; Sunagawa, Y.; Takahashi, H.; Muramatsu, A. *Chem. Commun.* **2005**, 348.
(6) Ekstrand, A.; Jansson, K.; Westin, G. *Chem. Mater.* **2005**, *17*, 199.
(7) Hou, Y.; Kondoh, H.; Ohta, T. *Chem. Mater.* **2005**, *17*, 3994.
(8) Tsang, S. C.; Caps, V.; Paraskevas, I.; Chadwick, D.; Thompsett, D. *Angew. Chem., Int. Ed.* **2004**, *43*, 5645.
(9) Afanasiev, P. *Inorg. Chem.* **2002**, *41*, 5317.

Table 1. Crystallographic Data[a] for $(NO_3)_2Me(H_2O)_6(HMTA)_2 \cdot 4H_2O$

	(**1**) Me = Co^{2+}	(**2**) Me = Ni^{2+}
refined formula	$C_{12}H_{44}Co_1N_{10}O_{16}$	$C_{12}H_{44}Ni_1N_{10}O_{16}$
fw (g mol^{-1})	643.5	643.2
cryst syst	triclinic	triclinic
unit cell constants		
a (Å)	9.1231 (3)	9.0976 (6)
b (Å)	9.4137 (5)	9.3448 (6)
c (Å)	9.6718 (4)	9.6909 (5)
α (deg)	88.214 (2)	87.779 (3)
β (deg)	75.600 (3)	75.679 (3)
γ (deg)	61.618 (2)	61.255 (3)
V (Å^3)	704.13 (6)	696.78 (8)
space group	$P\bar{1}$ (No. 2)	$P\bar{1}$ (No. 2)
Z	1	1
T (K)	293	293
density (g cm^{-3})	1.52	1.53
μ (mm^{-1})	0.695	0.782
R^b	0.0421	0.0453
$R_w{}^c$	0.0480	0.0475
S	1.12	1.15
$\Delta\rho_{max}$ (e Å^{-3})	0.59	0.51
$\Delta\rho_{min}$ (e Å^{-3})	−0.36	−0.33
no. of reflns used	2430	1724
no. of param	209	208

[a] All data collected with Mo Kα radiation ($\lambda = 0.710\,69$ Å). [b] $R = \sum(|F_o - F_c|)/\sum|F_o|$. [c] $R_w = \{\sum[w(|F_o - F_c|)^2]/\sum[w|F_o|^2]\}^{1/2}$.

metallic Ni- and Co-HMTA complexes led to the corresponding metals. A more detailed study of these systems revealed that both the initial compounds and decomposition products possess interesting properties, namely, the former are three-dimensional (3-D) supramolecular networks and the latter are metallic nanoparticles embedded within a porous carbon matrix. The present paper deals with the structural characterization of Ni- and Co-HTMA complexes and the properties of their decomposition products.

2. Experimental Section

Ni- and Co-HMTA complexes were obtained by aqueous reaction of the corresponding nitrates salts with HMTA. In a typical synthesis, 5.8 g of nickel (0.02 mol) or cobalt nitrate hexahydrate (0.02 mol) dissolved in 25 mL of distilled water was added to 25 mL of an aqueous solution containing 14 g of HMTA (0.1 mmol). Macroscopic platelike crystals (rose and light-green color for cobalt (**1**) and nickel (**2**), respectively) were filtered, washed with acetone, and dried in air (synthesis yield about 85%, not optimized).

Structure determination was carried out on a Nonius Kappa CCD diffractometer. The experimental details for the structure determination of $(NO_3)_2Me(H_2O)_6(HMTA)_2 \cdot 4H_2O$ (Me = Co^{2+}, Ni^{2+}) are given in Table 1. Once the data processing was performed by the Kappa CCD analysis softwares,[10] the lattice constants were refined by least-squares refinement using 2490 reflections ($1.0° < \theta < 28°$) for the cobalt compound and 2554 reflections ($1.0° < \theta < 28°$) for the nickel compound. No absorption correction was applied to the data sets. The structures were solved by direct methods (*SIR97* program[11]) combined with Fourier difference syntheses and refined against F using reflections with $I/\sigma(I) > 3$ (*CRYSTALS* program[12]). All important bond lengths and angles are summarized in Tables 2 and 3. For all of the non-H atoms, the agitation thermal factors

(10) Nonius. *COLLECT, DENZO, SCALEPACK, SORTAV*; Kappa CCD Program BV: Delft, The Netherlands, 1999.

(11) Cascarano, G.; Altomare, A.; Giacovazzo, C.; Guagliardi, A.; Moliterni, A. G. G.; Siliqi, D.; Burla, M. C.; Polidori, G.; Camalli, M. *Acta Crystallogr.* **1996**, *A52*, C-79.

Table 2. Important Bond Lengths and Distances for Compound **1**

Cobalt Environment					
Co1−O3	2.044(2)	Co1−O2	2.104(2)	Co1−O1	2.116(2)

Hydrogen Bonds				
donor	H	acceptor	donor−H−acceptor angle (deg)	H−acceptor distance
O2	H20	N5	154.7	2.016
O1	H11	N2	170.4	2.002
O2	H21	O8	156.3	2.009
O3	H31	O4	166.2	1.811
O4	H40	N4	172.6	1.940
O3	H30	N3	172.7	1.918
O4	H41	O5	173.4	1.923
O1	H10	O7	174.7	2.005
O5	H50	O6	171.7	1.928
O5	H51	O8	169.3	2.041

Table 3. Important Bond Lengths and Distances for Compound **2**

Nickel Environment					
Ni1−O3	2.022(2)	Ni1−O2	2.063(2)	Ni1−O1	2.063(3)

Hydrogen Bonds				
donor	H	acceptor	donor−H−acceptor angle (deg)	H−acceptor distance
O2	H20	N5	155.8	2.011
O1	H11	N2	162.3	2.013
O2	H21	O8	160.1	1.997
O3	H31	O4	166.4	1.797
O4	H40	N4	173.9	1.931
O3	H30	N3	165.2	1.944
O4	H41	O5	177.1	1.945
O1	H10	O7	167.8	2.000
O5	H50	O6	170.1	1.909
O5	H51	O8	165.8	2.030

were anisotropically refined. The H atoms of water molecules were found by Fourier differences and their positions refined.

The decomposition of compounds of cobalt (**1**) and nickel (**2**) was carried out in the temperature range 573–973 K under a nitrogen flow of 3 L h^{-1} with a heating rate of 5 K min^{-1}. Decomposition products were collected and kept under argon. The gaseous products evolved upon heating of the samples were studied using a mass spectrometer gas trace A (Fison Instruments) equipped with a quadrupole analyzer (VG analyzer) working in a faraday mode. The ionization was done by electron impact with an electron energy of 65 eV. The samples (ca. 0.1 g) were heated in a quartz cell at a heating rate of 5 K min^{-1}. A silica capillary tube heated at 453 K continuously bled off a proportion of the gaseous reaction products. Several signals were continuously registered, corresponding to molecular ions and fragments of H_2O, NO, N_2, CO, O_2, CO_2, and NO_2.

To characterize solid decomposition products, the X-ray diffraction (XRD) patterns were obtained on a Bruker diffractometer with Cu Kα emission. The diffractograms were analyzed using the standard JCPDS files. Chemical analyses were realized using the atomic emission method. Scanning electron microscopy (SEM) images were obtained on a Hitachi S800 device at the CMEABG Center of Lyon I Claude Bernard University. Transmission electron microscopy (TEM) micrographs were obtained on a JEOL 2010 device with an accelerating voltage of 200 keV. Specific surface areas and porosities were measured by low-temperature nitrogen adsorption and calculated by means of Brunauer−Emmett−Teller

(12) Watkin, D. J.; Prout, C. K.; Carruthers, J. R.; Betteridge, P. W. *CRYSTAL Issue 11*; Chemical Crystallography Laboratory: Oxford, U.K., 1999.
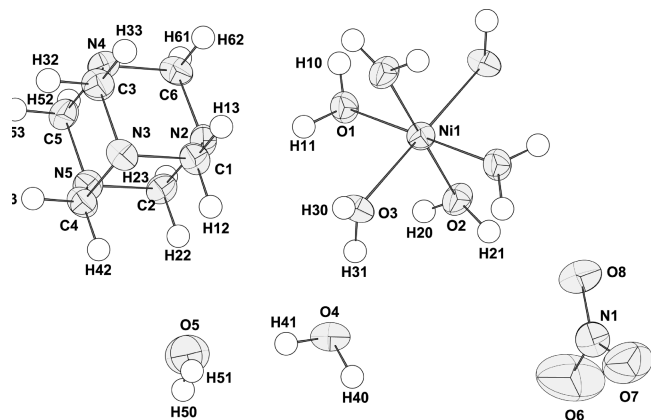
Figure 1. Illustration of the labeling for compounds **1** and **2**. Thermal ellipsoids are represented with a probability of 30%.

and Barrett−Joyner−Halenda equations. Adsorption measurements were performed on a Micromeritics ASAP2020 volumetric adsorption apparatus. Prior to measurement, the samples were degassed at 473 K for 4 h.

Extended X-ray absorption fine structure (EXAFS) experiments were carried out at the X1 beamline of the HASYLAB facility (Hamburg, Germany) using synchrotron radiation from the DORIS III ring. The Ni and Co K edges were monitored in the transmission mode, using a double Si(111) crystal monochromator. To characterize the metal environment evolution during heat treatments, a cell for in situ measurements was used. The cell was heated in an oven and crossed by the X-ray beam, while a nitrogen flow was maintained. The EXAFS data were treated with *FEFF*[13] and *VIPER*[14] programs. Then the edge background was extracted using Bayesian smoothing with a variable number of knots. The curve fitting was done alternatively in the R and k spaces, and the fit was accepted only in the case of simultaneous convergence in k and R spaces (absolute and imaginary parts for the latter). Coordination numbers (CNs), interatomic distances (R), Debye−Waller parameters (σ^2), and energy shifts (ΔE_0) were used as fitting variables. Constraints introduced relating to the fitting parameters were to obtain values at physically reasonable intervals. The quality of the fit was evaluated using the values of variance and goodness.

3. Results and Discussion

3.1. Structure of the Precursor Complexes. Macroscopic platelike crystals of Ni- and Co-HTMA complexes were spontaneously grown from aqueous solutions. The rose and light-green colors of the crystals for cobalt and nickel, respectively, were similar to the colors of the corresponding nitrates, indicating that no change of metal coordination occurred as a result of HMTA introduction. The results of chemical analysis suggest the stoichiometry $(NO_3)_2Me\text{-}(H_2O)_6(HMTA)_2 \cdot 4H_2O$ (with Me = Ni^{2+}, Co^{2+}), which fits perfectly with the single-crystal XRD results.

Both substances crystallize in the triclinic system, exhibit very close unit cell parameters (Table 1), and then present exactly the same structure. For clarity of the structural description of both compounds, the same labeling was used (Figure 1). Metal ions are placed in the inversion center and
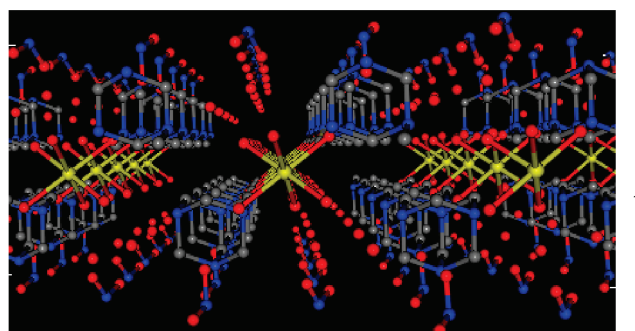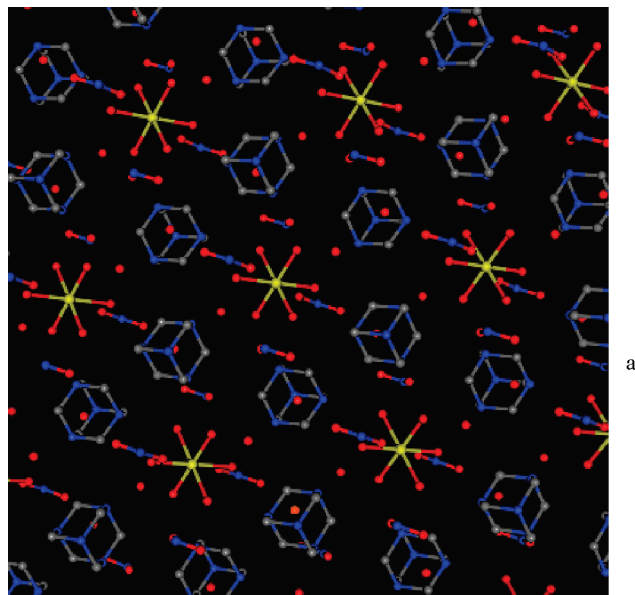
(13) Ankudinov, A. L.; Ravel, B.; Rehr, J. J.; Conradson, S. D. *Phys. Rev. B* **1998**, *58*, 7565.
(14) Klementiev, K. V. *J. Phys. D: Appl. Phys.* **2001**, *34*, 209. www.desy.de/~klmn/viper.html, *VIPER for Windows*, freeware.

Figure 2. Projection of the structural packing for both structures along the *c* axis of the unit cell. For clarity, H atoms have been omitted.
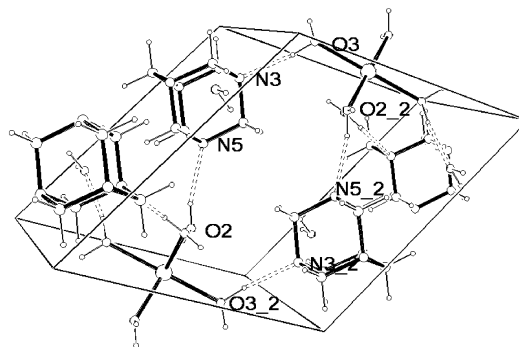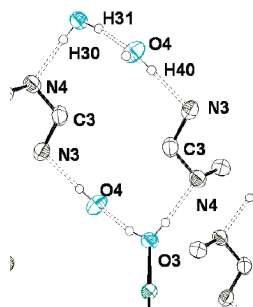

Figure 3. ORTEP graph showing the 16-membered hydrogen-bonded ring of the cationic network with participation of coordinated water. Nitrate groups and noncoordinated water molecules are removed for the presentation clarity.

are located in a perfect octahedral environment built from six water molecules (Table 2), with no more atoms being in special positions. As follows from the geometric parameters of the structure, HMTA is not bound to the metal, remaining outside the coordination shell. Adding to the $Me(H_2O)_6$ complex (with Me = Co or Ni) and HTMA, four free water molecules were found in the structure. Then, structural cohesion is assumed by hydrogen bonds building a 3-D network (Figures 2−4 and Tables 2 and 3). HMTA remains in the outer sphere probably because of its relatively low basicity.

Figure 4. ORTEP graph representing a R16 ring of hydrogen bonds with participation of noncoordinated water (O4).

While HMTA can formally be considered as an aliphatic amine (tetraazaadamantane), its complexing properties are much weaker than those of other polyamines such as ethylenediamine. At the same time, it belongs to the family of good proton acceptors for installing hydrogen bonds, as defined earlier by Donohue.[15]

The presence of four symmetrically placed N atoms and the overall cubic symmetry of the HMTA molecule allow the formation of up to four hydrogen bonds, thus generating hydrogen-bonded supramolecular frameworks. Indeed, supramolecular adducts of HMTA with organic and inorganic hydrogen-bonding donors have been described, such as layered bis(hexamethylenetetramine) diiodozinc(II)[16] or multiple helices and strings in the adducts with bisphenols and trisphenols.[17]

With the preparation technique being extremely simple, the complexes of HMTA with nickel and cobalt sulfate were prepared yet in 1982 by Ahuja et al., but no structural characterization was done.[18] Thermal analysis of the HMTA adducts to hydrated L_nCl_3 compounds $L_nCl_3 \cdot 0.2HMTA \cdot nH_2O$ (L = La, Pr, Nd, Sm, Dy, Er; n = 8, 10, 12) was reported by Zalewicz,[19] focused on the low-temperature dehydration processes. These nonexhaustive examples demonstrate a high ability of HMTA to produce supramolecular compounds with various H donors, including organic acids and metals of main and transition groups.

As shown in the analysis of hydrogen-bond connectivity in the structures of **1** and **2**, all N atoms of HMTA are involved in the hydrogen bonds, this creating a 3-D supramolecular assembly. Viewed along the [001] direction, the structure shows a hexagonal-like packing motif in which every $Co(H_2O)_6$ octahedron is surrounded by six HTMA molecules, which forms a trigonal antiprism. Perpendicular to [001], the structure can be alternatively represented as being lamellar, cationic layers and anionic layers of nitrates separated by HMTA (Figure 2). In the cationic layer, $R_4^4(16)$ rings[20] are formed by two hydrated Co ions and two HMTA molecules (Figure 3). Two types of such rings could be identified: one containing only coordinated water donors (O2

and O3) and another in which noncoordinated water participates (O4) together with coordinated water (O3) (Figure 4).

Nitrate anion molecules from different layers are connected through the coordinated water molecules, which creates chains interconnecting the adjacent HMTA layers along the z direction (−N1−O7−H10−O1−Co−O1− chain). At the same time, nitrate anions form standalone $R_4^2(12)$ rings within the anionic layers with participation of only noncoordinated water (−N1−O6−H50−O5−H51−O8− chain).

Interpenetration of these hydrogen-bonded patterns creates a 3-D framework. It would be interesting to study the nature of anionic and cationic moieties on the hydrogen-bonding trends in such HMTA-based supramolecular networks. Our preliminary tests (2001, unpublished work by P.A.) showed that, besides cobalt and nickel, other metals such as tin, cadmium, iron, and zinc are able to form well-crystallized complexes of the described type, whereas sulfate, acetate, chloride, and perchlorate may be involved in the anionic networks. Without much doubt, this list can be extended even more. It might be interesting to study how the metal coordination ability and/or anion properties influence the hydrogen bonding in such structures. Another possibility to construct supramolecular assemblies with participation of HMTA is to associate it with some metallic oxoanions. In this last case, ammonium or alkylammonium (but not tetraalkylammonium) is a convenient species to build up the cationic part of the network. An example of such a complex was the earlier described ammonium heptamolybdate−HMTA compound for which the unit cell was indexed but the structure is still not resolved.[9] Unfortunately, a more detailed discussion of this interesting topic is beyond the scope of the present work.

3.2. Decomposition Mechanism. As follows from the structural characterization, in the 3-D frameworks of compounds **1** and **2**, hydrated Co cations, and nitrate anions are separated in the layers by HTMA molecules. Therefore, decomposition upon heating is expected to proceed differently compared to that of cobalt nitrate (which gives Co_3O_4 as a solid product at ca. 500 K). We observed that decomposition of compounds **1** (cobalt complex) and **2** (nickel complex) in the temperature range 573−1073 K produced abundant black powder products. XRD patterns of the products indicate the formation of corresponding metals mixed with amorphous carbon. The differential thermal analysis curves showed somewhat different decomposition curves for nickel and cobalt compounds. The cobalt complex produced a very strong and narrow exothermic peak around 500 K, followed by a plateau of almost constant mass, whereas the nickel complex decomposed in several ill-resolved steps with total mass losses of 69 and 70 wt %, as can be seen in Figure 5. In both cases, the mass spectra of released gases indicate the formation of CO, ammoniac, some NO, and CH_2O (Figure 5a).

To explain high decomposition rates at relatively low temperatures, two factors should be taken into account. First of all, the presence of oxidizing nitrate and reducing HMTA may lead to ignition of the compound and its spontaneous decomposition as it occurs in the organic nitrates, although

(15) Donohue, J. *J. Phys. Chem.* **1952**, *56*, 502.
(16) Pickardt, J.; Droas, P. *Acta Crystallogr.* **1989**, *C45*, 360.
(17) Coupar, P. I.; Glidewell, C.; Ferguson, G. *Acta Crystallogr.* **1997**, *B53*, 521.
(18) Ahuja, I. S.; Yadava, C. L.; Singh, R. *J. Mol. Struct.* **1982**, *81*, 229.
(19) Zalewicz, M. *Thermochim. Acta* **1989**, *149*, 133.
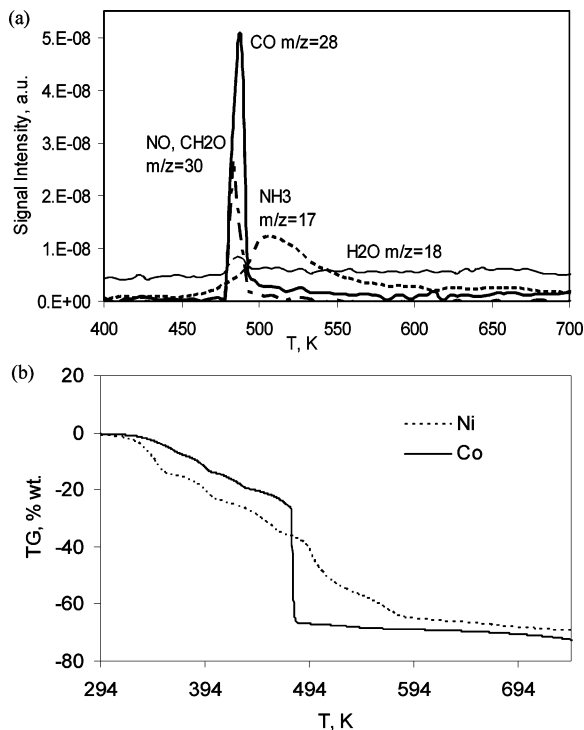(20) Etter, M. C. *Acc. Chem. Res.* **1990**, *23*, 120.

(a)

(b)

Figure 5. Mass spectra of gases evolved upon heating of a cobalt-containing complex in flowing argon, 5 K min⁻¹ (a), and thermogravimetric curves of decomposition at the same conditions for nickel- and cobalt-containing complexes (b).

much less violently, because of the presence of water and the very negative oxygen balance of these complexes. Second, cobalt is known to strongly accelerate decomposition of nitrate;[21,22] this might further increase the autocatalytic nature of the reactions involved.

The mass loss and the nature of gases produced allow for the proposal of the main decomposition pathway as follows:

$$(NO_3)_2Me(H_2O)_6(C_6H_{12}N_4)_2 \cdot 4H_2O \rightarrow Me + 6C + $$
$$10H_2O + 6CO + N_2 + 8NH_3 \quad (1)$$
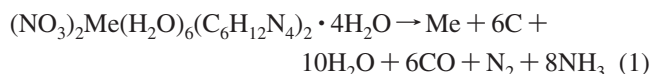
Besides this reaction, some secondary processes surely occur during decomposition, leading to some NO formation. As follows from the stoichiometry, all carbon cannot leave from the solids as CO, even if all oxygen is used to produce carbon oxide during decomposition. Indeed, in all specimens considerable amounts of residual carbon are detected. The calculated amount of carbon in the solid residual formed according to reaction (1) is 56%, whereas its real amount varied from 45 to 50% according to the specimen. Moreover, some oxygen is consumed to produce NO, unambiguously detected by mass spectrometry. At last, heavy organic residuals observed on the cold parts of the reactor after decomposition indicate that part of HMTA probably leaves the complex without reaction (by sublimation), which explains the deviation from the stoichiometry of reaction (1). However, reaction (1) seems to provide a good general description of the decomposition of complexes **1** and **2**.
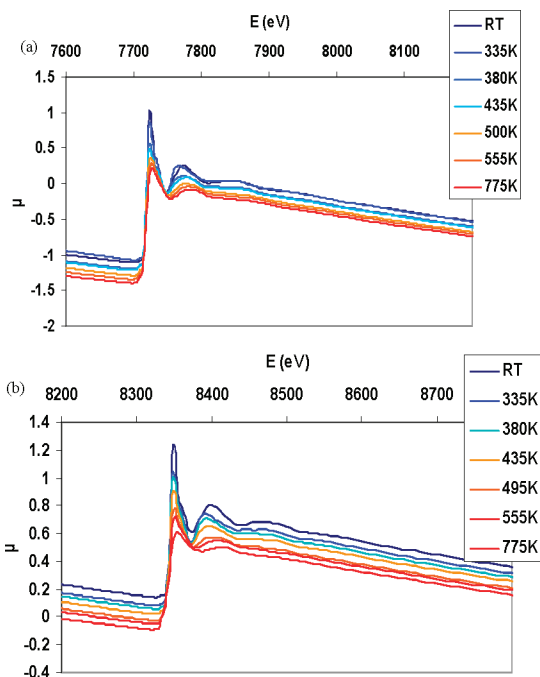
The Co and Ni K edges in the X-ray adsorption near-

(21) Xu, R.; Zeng, H. C. *Chem. Mater.* **2003**, *15*, 2040.
(22) Ehrhardt, C.; Gjikaj, M.; Brockner, W. *Thermochim. Acta* **2005**, *432*, 36.

Figure 6. In situ XAS spectra of the cobalt (a) and nickel (b) compounds upon their heating under a nitrogen flow.

edge structures (XANES) region of compounds **1** and **2** heated under nitrogen at different temperatures are shown in Figure 6. For both solids, the edge shape was changed in the same way from the initial substance to the products of heating. The characteristic white line attributed to cobalt and nickel in the oxygen environment was present in the initial solids but decreased upon heating, which indicates an increase of the electron population in the cobalt (nickel) third level. Thus, we infer from the XANES part of the spectra that the cobalt and nickel coordination changed from the oxygen octahedra in the **1** and **2** precursors to the disordered and partially reduced states already at relatively low temperatures.

Analysis of the in situ EXAFS spectra as a function of the heating temperature reveals fine details of the decomposition mechanism. For both metals, evolution is similar, but this issue can be better illustrated by Ni K spectra because in the case of nickel the evolution is smoother. In the initial **1** and **2** compounds, the most important peaks on the Fourier transform (FT) of EXAFS spectra correspond to those expected from the structures of six oxygen neighbors (Figure 7). Because there are no close-standing heavy neighbors in the structure, the EXAFS spectra can be fairly well described by these first six oxygen shells of the hydrated $M(H_2O)_6^{2+}$ ions (Table 4), with the contribution from HMTA and nitrate being less important. After heating to 373 K, the position of this main peak virtually does not change but the intensity decreases twice (losing crystallinity). At the same time, some new and far-standing heavy (nickel and cobalt) neighbors begin to appear, which are very positionally disordered (see Debye–Waller factor estimations in Table 4). This situation corresponds to the loss of crystallographic water and the solid amorphization. At this stage of 10–20% weight loss, the onset
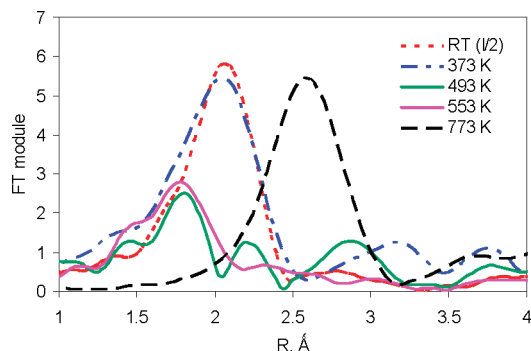
Figure 7. FT module of the EXAFS spectra, measured in situ upon heating of compound **2** under nitrogen at different temperatures.

Table 4. Evolution of the Coordination State of Nickel during Heating of Compound **2** under Nitrogen, as Inferred from the Ni K Edge EXAFS Fit Results

atom type	R (Å)	N	σ^2 (Å^2)	ΔE_0 (eV)
		Initial **2**		
O	2.05(1)	5.7(4)	0.007(1)	−1.0(4)
		373 K		
O	2.06(2)	4.2(5)	0.009(2)	−1.0(4)
Ni	3.14(3)	5.2(5)	0.030(5)	−1.0(4)
Ni	3.64(5)	4.2(5)	0.022(7)	−1.0(4)
		493 K		
C	1.81(2)	4.5(3)	0.008(1)	−2.0(4)
O	2.21(2)	2.3(2)	0.008(1)	−2.0(4)
Ni	2.82(2)	3.5(5)	0.008(1)	−2.0(4)
		553 K		
C	1.83(2)	4.1(5)	0.015(5)	−3.2(4)
Ni	2.42(2)	2.1(5)	0.021(7)	−3.2(4)
		773 K		
C	1.82(3)	0.2(1)	0.020(5)	−3.0(5)
Ni	2.42(3)	5.5(2)	0.008(1)	−3.0(5)

of structure collapse is evident and probably Co (Ni) atoms become closer.

A very important change of the metal environment occurs suddenly near the main weight loss temperature, 493 K. At the level of ca. 40% weight loss, the oxygen peak near 2.0 Å disappears and leaves in its place two new types of neighbors at 1.81 and 2.21 Å. The first one can be attributed to carbon because among the elements involved only carbon may provide such a short interatomic distance with nickel. The second type of neighbor at 2.21 Å is presumably the residual oxygen, which completes the coordination shell of the metal, its CN remaining close to six. While this drastic change occurs, the far-standing metal neighbor shifts to 2.8 Å; i.e., it continues to come closer to the central atom.

Soon after the main weight loss (523 K), the remaining oxygen leaves and the metal−metal distance appears, close to that in the bulk metal. Carbon still remains the main element in the coordination shell. However, upon further heating (573 K and further), the coordination rapidly evolves toward that of the bulk metal. At 777 K, no presence of carbon neighbors could be reliably inferred from the EXAFS spectrum fitting.

Overall, the in situ EXAFS experiments demonstrate that the decomposition occurs via the intermediate amorphous product in which nickel (cobalt) has mostly carbide-like coordination. However, the crystalline structure of the only known carbide Ni$_3$C predicts only two carbon neighbors for

the Ni atom,[23] whereas we observe about four C atoms. Even for the relatively low precision of CN determination from EXAFS, this is a very significant difference. Therefore, we cannot postulate any structural relationship between the known nickel and cobalt crystalline carbides and the amorphous carbide that we observe by EXAFS. It seems rather that Ni and Co atoms are embedded into the amorphous carbonaceous matrix. This can be expected from the large excess of carbon, in both the precursor and the decomposition products.

In any case, both experimental and theoretical data suggest the instability of existing nickel and cobalt carbides and their decomposition to carbon and the corresponding metals. Indeed, Goodman et al.[24] studied the kinetics of Ni$_3$C transformations using Auger spectroscopy and observed very rapid decomposition of Ni$_3$C with th eformation of graphite at 700−800 K. Density functional theory calculations also corroborated the metastability of nickel and cobalt carbides. The formation energy of Ni$_3$C calculated with respect to bulk nickel or cobalt and graphite is positive; i.e., the M$_3$C phases are metastable or unstable at ambient conditions.[25] These results are in line with our observations.

3.3. Characterizations of the Decomposition Products. Core−shell magnetic particles are presently a hot research topic. Indeed, metal−carbon composite materials are attractive for several applications including magnetic materials,[26–28] supercapacitors,[29] and catalysts[30] and for electrochemical applications.[31,32] For some of these applications, carbon-encapsulated metal particles represent the most desirable form of a metal−carbon composite material. These include magnetic materials and magnetically separable adsorbents and/or catalysts in which the carbon surface is exposed while magnetic metal nanoparticles are protected by the carbon shell. Because of such a core−shell structure, these materials possess high chemical stability,[33] while nonprotected carbon-supported metals particles are easily oxidized even at low temperatures.[34]

Owing to these advantageous properties, various methods for synthesis of the core−shell carbon-encapsulated nano-

(23) Nagakura, S. *J. Phys. Soc. Jpn.* **1958**, *13*, 1005.
(24) Goodman, D. W.; Kelley, R. D.; Madey, T. E.; White, J. M. *J. Catal.* **1980**, *64*, 479.
(25) Shein, I. R.; Medvedeva, N. I.; Ivanovskii, A. L. *Physica B* **2006**, *371*, 126.
(26) Fonseca, F. C.; Ferlauto, A. S.; Alvarez, F.; Goya, G. F.; Jardin, R. F. *J. Appl. Phys.* **2005**, *97*, 044313.
(27) Wang, H.; Wong, S. P.; Cheung, W. Y.; Ke, N.; Chiah, M. F.; Liu, H.; Zhang, X. X. *J. Appl. Phys.* **2000**, *88*, 2063.
(28) Dravid, V. P.; Host, J. J.; Teng, M. H.; Elliott, B. R.; Hwang, J. H.; Johnson, D. L.; Mason, T. O.; Weertman, J. R. *Nature* **1995**, *374*, 602.
(29) Li, W.; Reichenauer, G.; Fricke, J. *Carbon* **2002**, *40*, 2955.
(30) Rodríguez-Reinoso, F. Carbon as catalyst support. In *Porosity in Carbons*; Patrick, J. W., Ed.; Wiley: Oxford, U.K., 1995; p 253.
(31) Alcántara, R.; Lavela, P.; Ortiz, G. F.; Tirado, J. L.; Stoyanova, R.; Zhecheva, E.; Mateos, J. M. J. N. *J. Electrochem. Soc.* **2004**, *151*, A2113.
(32) Alcántara, R.; Lavela, P.; Ortiz, G. F.; Tirado, J. L.; Stoyanova, R.; Zhecheva, E.; Merino, C. *Carbon* **2004**, *42*, 2153.
(33) Lu, A. H.; Li, E. C.; Matoussevitch, N.; Spliethoff, B.; Bönnemann, H.; Schüth, F. *Chem. Commun.* **2005**, 98.
(34) Chernavskii, P. A.; Pankina, G. V.; Chernavskii, A. P.; Peskov, N. V.; Afanasiev, P.; Perov, N. S.; Tennov, V. A. *J. Phys. Chem. C* **2007**, *111*, 5576.

particles have been developed, including high-temperature techniques such as arc discharge[35,36] of chemical vapor depositions.[37,38] Although these methods have succeeded in synthesizing carbon-encapsulated transition metals, the high-temperature process of the methods hinders the preparation of the carbon-encapsulated nanoparticles of the metastable phase and low-melting-point metals.

To decrease the preparation temperature, decomposition of molecular precursors has been studied, for example, carbon-encapsulated iron by pyrolysis of ferrocene in pure hydrogen.[39] Other examples include the preparation of cobalt nanoparticles from the [bis(salicylidene)cobalt(II)]−oleylamine complex by thermal decomposition[40] and acetylide decomposition, leading to encapsulated cobalt, nickel, and palladium.[41] Combined techniques were also reported such as two-step preparations including the glycothermal preparation of metal nanoparticles followed by carbonization.[42]

Investigation of the morphology of the decomposition products using electron microscopy and surface area measurements reveals that these are solids with open pores and high specific surface areas (190 m^2/g for cobalt and 165 m^2/g for nickel, both obtained at 823 K). A spongelike morphology is characteristic for all of the specimens studied. A similar morphology was found for nickel- and cobalt-containing specimens, whatever the final temperature, provided it was higher than 673 K. Probably, the morphology is determined by decomposition, which occurred rapidly at relatively low temperature. In this case, the heating rate and the final temperature should be of less importance.

Like any foams, the solids obtained are fractal structures with polymodal pore distributions. Low-temperature nitrogen adsorption–desorption isotherms showed very broad pore-size distributions with pronounced mesoporosity and macroporosity features (Figure 8). At the same time, the nitrogen desorption isotherms suggest a relatively small share of the microporosity in the total pore volume, though the latter is often observed in the carbon-based materials obtained from pyrolysis[43] of organics. High surface area and large pore size for the preparations reported here are probably related to the large amount of gases produced during the decomposition. From the six kinds of adsorption isotherms by IUPAC classification,[44] the solids are meso- and macroporous showing type II shape. In the low-pressure region, the isotherms have inflection points at relative pressures of less than 0.05. At these points, samples have absorbed only about 20 cm^3/g of nitrogen. Then, in the intermediate domain, the adsorbed volume increases almost linearly. Over the relative
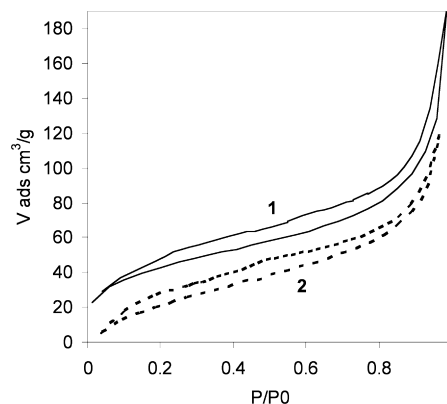
Figure 8. Nitrogen adsorption–desorption isotherms for the cobalt (**1**) and nickel (**2**) solids after heating at 773 K. For presentation convenience, the curve of **2** was shifted down by a value of 20 cm^3/g.
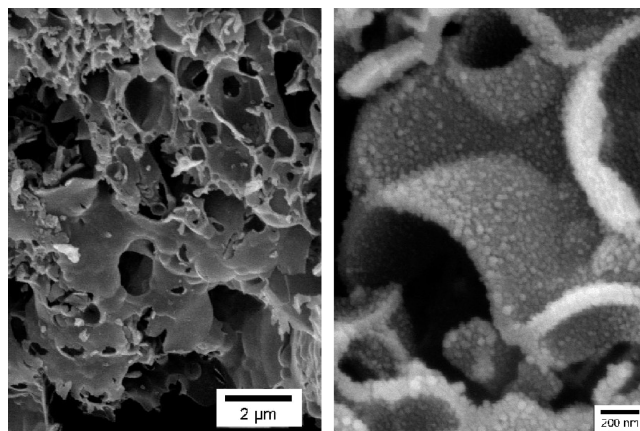
Figure 9. SEM images of the metal–carbon composite foam obtained by the decomposition of the nickel complex (**2**) at 823 K. Images were taken at magnification 6000 (left, a) and 40 000 (right, b).

pressure 0.7–0.8, the isotherms demonstrate sharp slopes, indicating that they contain macrospores. The micropore volume percentage of the total pore volume in both samples was less than 15–20%.

At the same time with mesopores accessible by nitrogen adsorption, spherical open macropores of different size ranging approximately from 100 nm to 1 μm were observed straightforwardly by SEM (Figure 9). The energy-dispersive X-ray (EDX) analyses coupled with SEM and TEM observations confirm that the grains correspond to metals, whereas the surrounding matter is carbonaceous. Metal particle sizes are similar for cobalt and nickel, with nickel grains slightly larger and more anisotropic. Visual inspection of TEM images gives the value between 10 and 20 nm (Figures 10 and 11). Statistical treatment of representative images for the specimens heated at 773 K (Figure 12a) shows rather narrow particle size distribution centered at 12 nm. The distribution is not symmetric, which is expected for a kinetically controlled process.

The final temperature does not strongly influence the particles size. This was inferred from the comparison of two XRD patterns of cobalt-containing solids, heated at 773 and 1073 K, respectively (not shown). As follows from Scherrer calculations, an increase of the heating temperature by 300 K led only to a modest particle size increase from 6.6 to 8

(35) Scott, J. H. J.; Majetich, S. A. *Phys. Rev. B* **1995**, *52*, 12564.
(36) Huo, J.; Song, H.; Chen, X. *Carbon* **2004**, *42*, 3177.
(37) Flahaut, E.; Agnoli, F.; Sloan, J.; O'Connor, C.; Green, M. L. H. *Chem. Mater.* **2002**, *14*, 2553.
(38) Wang, Z. H.; Choi, C. J.; Kim, B. K.; Kim, J. C.; Zhang, Z. D. *Carbon* **2003**, *41*, 1751.
(39) Sano, N.; Akazawa, H.; Kikuchi, T.; Kanki, T. *Carbon* **2003**, *41*, 2159.
(40) Salavati-Niasari, M.; Davar, F.; Mazaheri, M.; Shaterian, M. *J. Magn. Magn. Mater.* **2008**, *320*, 575.
(41) Nishijo, J.; Okabe, C.; Oishi, O.; Nishi, N. *Carbon* **2006**, *44*, 2943.
(42) Zhu, G. X.; Wei, X. W.; Jiang, S. *J. Mater. Chem.* **2007**, *17*, 2301.
(43) Steel, K. M.; Koros, W. J. *Carbon* **2005**, *43*, 1843.
(44) Sing, K. S. W.; Everett, D. H.; Haul, R. A. W.; Moscou, L.; Perotti, R. A. *Pure Appl. Chem.* **1985**, *57*, 603.
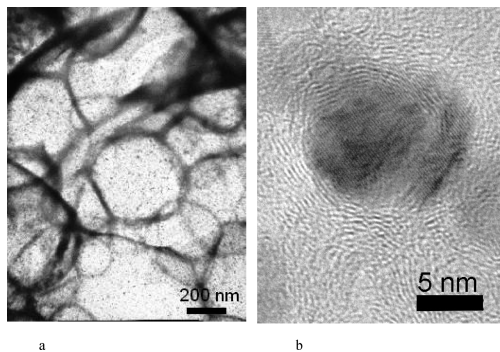
Figure 10. TEM images of the metal–carbon composite foam obtained from the nickel complex (**2**) at magnification 50 000 (a) and a stand-alone particle encapsulated within lamellar carbonaceous matter (b).
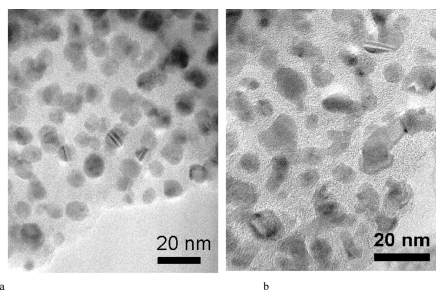

Figure 11. Representative TEM images of solids **1** (a) and **2** (b) after heating at 773 K, used for the statistical determination of the particle size.
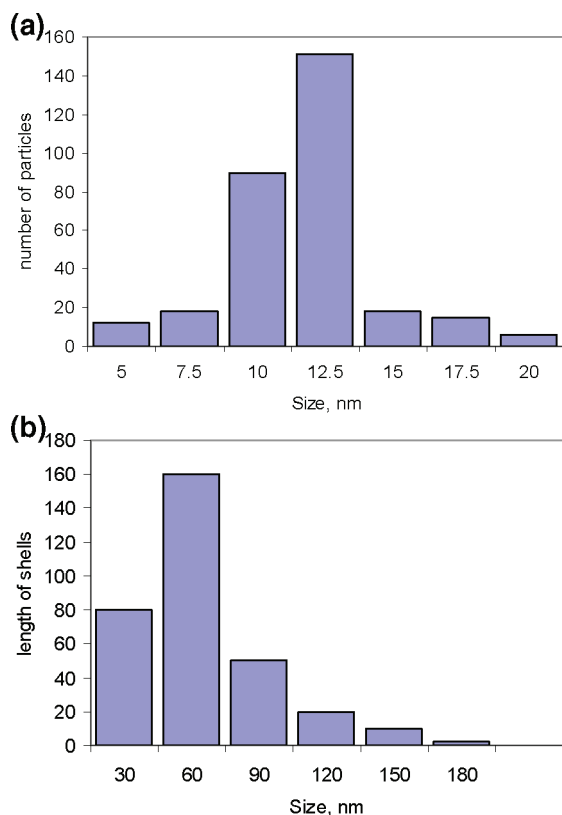

Figure 12. Size distribution histogram for particles obtained from the decomposition of **2** at 773 K (a) and distribution of the shell thickness in the same sample (b).

nm. Note that calculation of the particle size from the XRD patterns using the Scherrer formula gave an average size somewhat smaller than the results of the TEM study. While TEM yielded real size distribution statistics for each sample, the XRD Scherer analysis led to a "mean" particle size. This discrepancy is well documented and was attributed to the different weightings inherent in the use of XRD.[45]

Inspection of the SEM and TEM images for the **1** and **2** decomposition products leads to that conclusion that for any heating temperature the pore walls have a very broad distribution of thicknesses between 10 and 500 nm, with the maximum of distribution at ca. 60 nm (Figure 12b). Compared to the particle size, the mean wall thickness is significantly greater. The metal particles are arranged within the pore walls, and analysis of the tilted images suggests that there are almost no contacts between the particles (Figure 10b). This partially explains the high stability of the particle size to the heating. At the same time, high-resolution TEM shows that the metal particles are covered with onionlike carbon shells. These carbon shells probably have a stabilizing effect on the particles size, which remained nearly constant when the final decomposition temperature was increased. Our preliminary studies show that the materials have a saturation magnetization of about 50 emu/g in the case of cobalt. The materials withstand heating in air to 500 K without a significant magnetization drop. As with the oxidation stability under ambient conditions, it is worth noting that these materials, first prepared by one of the authors in 2001 (see ref 9) and stored in air, still keep virtually the same magnetization values as freshly prepared solids.

4. Conclusions

Cobalt and nickel are very important metallic materials, with a wide range of applications related to their catalytic and magnetic properties. However, there are quite a few efficient methods to produce porous solids of high surface area. Modifications of the Raney technique remained until recently the most frequently used approach to the preparation of these metals in a highly dispersed state appropriate for adsorption and catalysis. However, in the last few years, a boost of research activity was observed on the preparation of nanoscopic nickel and cobalt, using various physical or chemical methods.[46–48]

For the preparations described here, the important point is that the newly synthesized molecular precursors are simple compounds with definite structure. This allows avoidance of any uncertainty in the processing stages prior to the preparation of metal nanoparticle foams. HMTA is an easily available compound produced by the reaction of ammonia with formaldehyde. HMTA is very cheap and nontoxic unlike many other precursors such as aliphatic (di)amines. This makes our approach as environmentally friendly as possible for these types of materials (any nickel and cobalt compounds

(45) Ashcroft, A. T.; Cheetham, A. K.; Harris, P. J. F.; Jones, R. H.; Natarajan, S.; Sankar, G.; Stedman, N. J.; Thomas, J. M. *Catal. Lett.* **1994**, *24*, 47.

(46) Sergiienko, R.; Shibata, E.; Zentaro, A.; Shindo, D.; Nakamura, T.; Qin, G. *Acta Mater.* **2007**, *55*, 3671.

(47) Singjai, P.; Wongwigkarn, K.; Laosiritaworn, Y.; Yimnirun, R.; Maensiri, S. *Curr. Appl. Phys.* **2007**, *7*, 662.

(48) Baranauskas, V. V.; Zalich, M. A.; Sanders, M.; St. Pierre, T. G.; Riffle, J. S. *Chem. Mater.* **2005**, *17*, 5246.

are toxic by definition). The precursor's preparation occurs in one step in an aqueous solution at ambient conditions. Therefore, this method using simple and cheap precursors seems suitable for large-scale production of catalysts or magnetic materials.

Because of the presence of a high amount of nitrogen and some oxygen in the precursor, large amounts of gaseous water, CO, and nitrogen are formed during the decomposition. Exothermal interaction of nitrate with amine leads to a strong gas dilatation, and the foam is formed. The foam produced possesses a highly porous structure.

The precursors are highly soluble in water (though less than the initial nitrate), and the solution is stable. Evaporation leads to the reprecipitation of the precursor. Therefore, the magnetic foam can be obtained within any template with appropriate cavities by simple heating of an impregnated solid.

Supporting Information Available: X-ray crystallographic data in CIF format. This material is available free of charge via the Internet at http://pubs.acs.org.

IC7013013